Earth Planets Space, **53**, 1011–1019, 2001

Visualization and criticality of magnetotail field topology in a three-dimensional particle simulation

DongSheng Cai[1], Yaoting Li[1], Taizi Ichikawai[1], Chijic Xiao[1], and Ken-ichi Nishikawa[2]

[1]*Institute of Information Sciences and Electronics, the University of Tsukuba, 1-1-1 Ten-nou-dai, Tsukuba 305-8573, Japan*
[2]*Department of Physics and Astronomy, Rutgers University*

(Received July 9, 2000; Revised July 7, 2001; Accepted July 10, 2001)

We present the temporal evolution of magnetic field topology in the magnetotail with a southward IMF in order to identify the magnetic reconnection. The magnetic field topology is uniquely determined by the eigenvalues of the critical points, if they are not degenerated. This is because the critical points, their number, and the rules between them characterize the whole magnetic field pattern. At the critical points, the magnetics become zero. The magnetic vector field curves and surfaces are both integrated out along the principal directions of certain classes of critical points including the Earth's dipole magnetic field. The skeleton that includes the critical points, characteristic curves, and surfaces provides the three-dimensional topological structure of the reconnection. The change of the skeleton, i.e. the change of the topology, has revealed the occurrence of magnetic reconnection. Namely, three-dimensional "X-points" or the more-than-two critical points that are saddle and connected each other are unstable and can move, vanish, and generated.

1. Introduction

Three-dimensional magnetic field topology in magnetosphere represents a domain of space plasma physics of great interest that is, as yet, beyond the reach of definitive theoretical analysis or numerical computations. At present, our understanding of three-dimensional magnetic field rests principally on observations drawn from experimental satellite data or some global simulations of the Earth magnetosphere.

On the other hand, when computer graphics were introduced as a field of study, the visualization techniques based on it were closely resemble to the "pictures" that were already in use in the field. The researchers who had examined thousands of them, have recognized that images that actually contain more information are useful than new presentations. However, direct visualization methods in which thousands of points, vectors or curves are displayed are inadequate to visualize many complex data sets. Furthermore, manually choosing a smaller set of elements for direct display is usually both time-consuming and misleading.

Our research was motivated by the importance of topology in order to understand the dynamics of magnetic field in the magnetotail. We have noticed that it is difficult to understand the topology in the complex magnetic fields with the existing tools. In this paper, we present some methods that automate the analysis and display magnetic field topology in the near Earth, especially in the magnetotail where the magnetic reconnection occurs. First, we describe the basis of critical point analysis and classifications, and the three-dimensional algorithm of our visualizations. Second, we visualize the three-dimensional magnetic field topology in the magnetotail in order to reveal the global change of topology. The visualizations are based on the numerical data sets obtained by the three-dimensional electromagnetic particle simulation (Nishikawa, 1997, 1998a).

Topology provides useful information on the entire magnetic field structure with the simplified magnetic fields displayed by the critical points and surfaces based on the eigenvalues, which will be discussed later. Critical points of the field can be categorized mathematically. Thus the types of critical points, their number, and the rules governing the relations among them can characterize the magnetic field pattern. Magnetic reconnections in this view have been defined by the change of this structure following the rules governing the relations among them. However, this view of reconnections is not universally accepted, and requires further investigation.

2. Critical Points

Critical points or magnetic nulls are the points where the magnitude of magnetic field vector vanishes. These points may be characterized by the behavior of nearby magnetic field curves or surfaces. The set of curves or surfaces which end on the critical points is of special interest because it defines the behavior of the magnetic field in the neighborhood of the critical point. If all the eigenvalues of critical points in the region where we consider are hyperbolic, then the magnetic vector field topologies are uniquely determined only by the critical points, the magnetic field curves, and surfaces that are originated from the critical points (Arnold, 1981). The usual magnetic field configuration satisfies the hyperbolic conditions. Thus the particular sets of the critical points, curves, and surfaces can be used to define a skeleton

that uniquely characterizes the magnetic field.

For simplicity, we use $\mathbf{v} = (u, v, w)^t$ instead of $\mathbf{B} = (B_x, B_y, B_z)^t$ as the magnetic vector field. First we expand the magnetic vector field $\mathbf{v}(x, y, z)^t$ around the critical point $\mathbf{x} = (x_0, y_0, z_0)^t$ to the first order:

$$\begin{aligned}\mathbf{v} &= \frac{d\mathbf{x}}{dt} \\ &= \begin{pmatrix} u(x_0, y_0, z_0) \\ v(x_0, y_0, z_0) \\ w(x_0, y_0, z_0) \end{pmatrix} \\ &+ \begin{pmatrix} \frac{\partial u}{\partial x} & \frac{\partial u}{\partial y} & \frac{\partial u}{\partial z} \\ \frac{\partial v}{\partial x} & \frac{\partial v}{\partial y} & \frac{\partial v}{\partial z} \\ \frac{\partial w}{\partial x} & \frac{\partial w}{\partial y} & \frac{\partial w}{\partial z} \end{pmatrix} \begin{pmatrix} x - x_0 \\ y - y_0 \\ z - z_0 \end{pmatrix} \\ &+ \mathbf{O}(2). \end{aligned} \tag{1}$$

Here we know that $\begin{pmatrix} u(x_0, y_0, z_0) \\ v(x_0, y_0, z_0) \\ w(x_0, y_0, z_0) \end{pmatrix} = \begin{pmatrix} 0 \\ 0 \\ 0 \end{pmatrix}$, and

$$\mathbf{J} = \begin{pmatrix} \frac{\partial u}{\partial x} & \frac{\partial u}{\partial y} & \frac{\partial u}{\partial z} \\ \frac{\partial v}{\partial x} & \frac{\partial v}{\partial y} & \frac{\partial v}{\partial z} \\ \frac{\partial w}{\partial x} & \frac{\partial w}{\partial y} & \frac{\partial w}{\partial z} \end{pmatrix}, \mathbf{x} = \begin{pmatrix} x - x_0 \\ y - y_0 \\ z - z_0 \end{pmatrix}. \tag{2}$$

Thus we get the linearized form of the magnetic vector field:

$$\frac{d\mathbf{x}}{dt} = \mathbf{J}\mathbf{x}. \tag{3}$$

Here to the first order approximation, a critical point can be classified according to the eigenvalues of the Jacobian matrix $\mathbf{J}$ of the vector $\mathbf{v}$ with respect to the critical point $\mathbf{x}$:

$$\left.\frac{\partial(u, v, w)}{\partial(x, y, z)}\right|_{x_0, y_0, z_0} = \left.\begin{pmatrix} \frac{\partial u}{\partial x} & \frac{\partial u}{\partial y} & \frac{\partial u}{\partial z} \\ \frac{\partial v}{\partial x} & \frac{\partial v}{\partial y} & \frac{\partial v}{\partial z} \\ \frac{\partial w}{\partial x} & \frac{\partial w}{\partial y} & \frac{\partial w}{\partial z} \end{pmatrix}\right|_{x_0, y_0, z_0}. \tag{4}$$

Figure 1 shows how the eigenvalues classify a critical point as an attracting node (7), a repelling node (6), an attracting focus (5), a repelling focus (3), and four saddles (1), (2), (4), and (8). It should be noted that a positive or negative real part of an eigenvalue indicates an attracting or repelling nature, respectively. The nonzero imaginary part create a spiral structure around the critical points. The saddle points are distinguished by the characteristic magnetic Σ-surfaces that are spanned by the two eigenvectors that have the same sign of real parts of eigenvalues as will be shown later. The two outgoing or incoming eigenvectors span the Σ-surfaces.

In our magnetic vector field unlike the electric vector field we have the solenoidal condition $\nabla \cdot \mathbf{B} = 0$. Thus three eigenvalues of the critical point $\lambda_1, \lambda_2, \lambda_3$ have to satisfy the condition

$$\lambda_1 + \lambda_2 + \lambda_3 = 0. \tag{5}$$

All the eigenvalues cannot be all positive or negative. Therefore, the four types of saddle point satisfy the condition as shown in Fig. 2. According to the notation used in Lau and

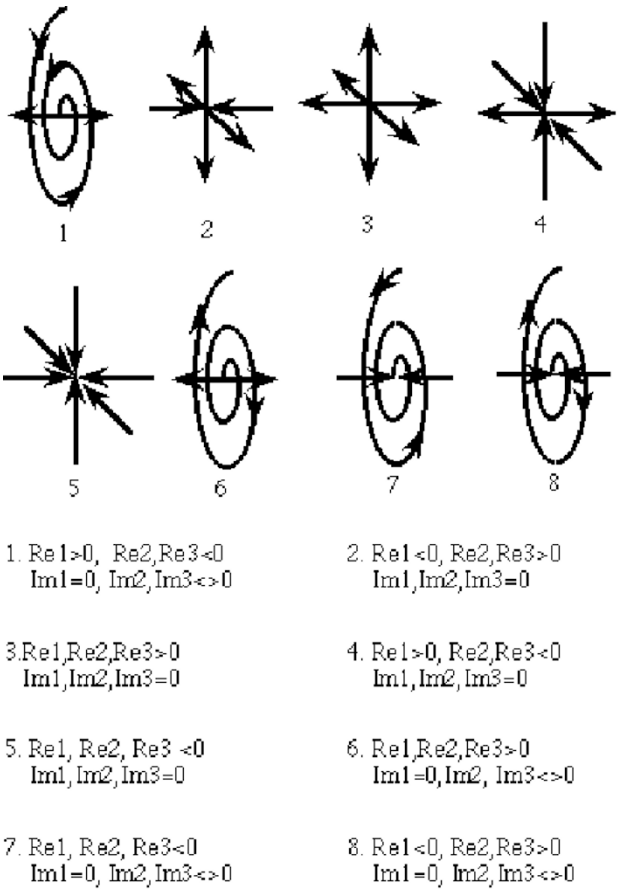

Fig. 1. Classification of critical points in three-dimension.

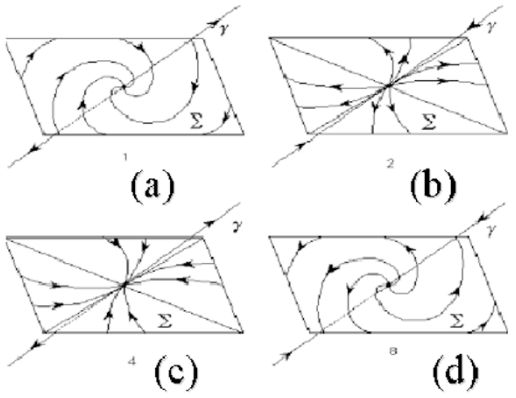

Fig. 2. Classification of saddle points. (a) type A_s, (b) type B, (c) type A, and (d) type B_s.

Finn (1990), if two of the real parts of the eigenvalues are negative, we call the critical point type A. Otherwise, we call the critical point type B. If the imaginary parts of eigenvalues are not zero, we call type A and type B critical points as type A_s and type B_s, respectively, as shown in Fig. 2. In three-dimension, for the simplest case that is the case both Σ-surfaces are plane, both type A (or A_s) and type B (or B_s) are connected together or paired, which forms the

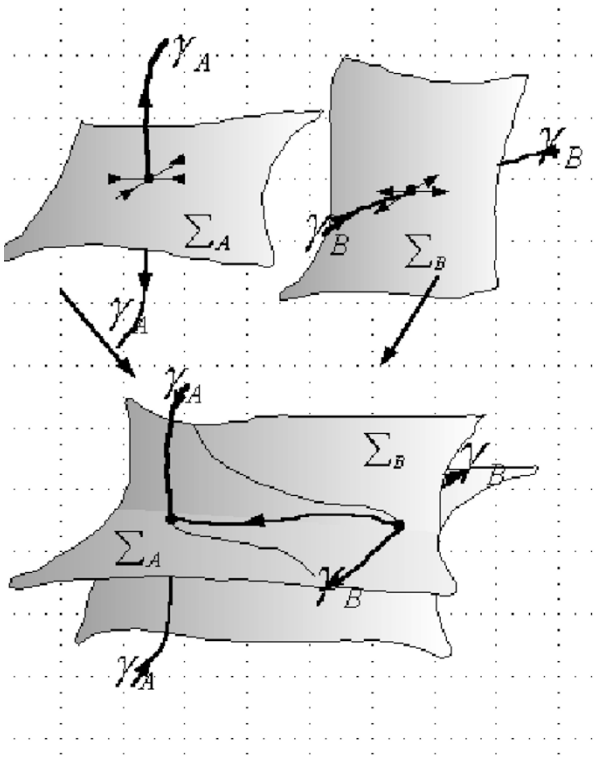

Fig. 3. Three-dimensional "X-point." Type A and type B merge and form a three-dimensional "X-point."

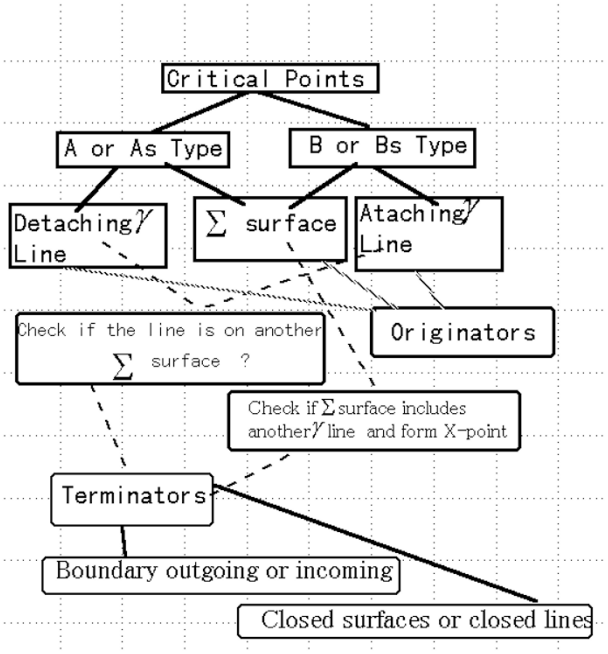

Fig. 4. Classification of critical points and visualization algorithms. The characteristic surfaces determined and extended from types A, B, A_s, and B_s critical points can be decomposed into γ-lines and Σ-surfaces, which form the skeleton magnetic fields in three-dimensions.

three-dimensional "X-point" as shown in Fig. 3. Note that in this figure the Σ-surfaces are assumed to be planes. The Σ-surfaces can be any two-dimensional manifolds including a plane, a cylinder, etc. The types of critical points, their number, and the rules governing the relations among them can characterize the whole magnetic field pattern. This schematic picture gives us the unique global skeleton of the magnetic field topology, which means all other magnetic fields are topologically equivalent. Please note that the algorithms of our visualization technique are summarized in Fig. 4. The manifolds that are determined and extended from the critical points can be decomposed into γ-lines and Σ-surfaces that are one and two-dimensional manifolds, respectively. These mixed manifolds based on the eigenvectors form the skeleton of magnetic field topology, which uniquely determines the topology of the magnetic field. In reality, the visualization of three-dimensional vector field is not so easy as one may expect, since the surfaces are integrated and extended from the critical points. Thus if they extend further in space, the numerical errors accumulate more. In addition, the Σ-surfaces may not always be plain surfaces and can be of any two-dimensional manifolds and form complicated three-dimensional "X-points." The types of critical points, their number, and the rules governing the relations among them characterize the magnetic field structure. The types of the two-dimensional manifold also are related to this rule. In this algorithm, we need to find multiple-connected pairs of type A and type B critical points. We also need to find that the γ-lines are on the different Σ-surfaces and thus more than two critical points form three-dimensional "X-points." However, the problem is that the "X-points" in the magnetotail are not like a simple three-dimensional "X-point" as shown in Fig. 3. The type A and type B critical points are multiple-connected and the Σ-surface is not always a plane surface and rather a cylinder or nose cones. The complicated three-dimensional "X-points" and their temporal changes in topology will be discussed in the next section using numerical data set from TRISTAN code. The topology rules between the critical points must be satisfied globally. Thus, in Fig. 4, some γ-lines and Σ-surfaces can be terminated as the "boundary outgoing or incoming" and satisfy the rules between them including the condition outside. In the present paper, we visualize the magnetic field topology only in the magnetotail region because the whole simulation domain is too large to visualize. In the TRISTAN simulation, the interplanetary magnetic field is included on the boundary with the IMF. In our paper, the term "local" refer to the phenomena where the critical points must satisfy the topology rules in the local region, for example, the region inside earth magnetosphere. The term "global" refer to the phenomena that the critical points must satisfy the topology rules not only in the local, but in the outside where the IMF exists. In brief, the term "global" means non-"local."

3. Visualizing Magnetotail Field Topology in a Three-Dimensional Particle Simulation

We visualize the magnetic field topology in the magnetotail using the data sets obtained by the three-dimensional full electromagnetic particle simulation with a southward IMF (Nishikawa, 1997, 1998a). For the simulation of solar wind-magnetosphere interactions, the following boundary conditions were used for the particles (Buneman *et al.*, 1993, 1995; Nishikawa *et al.*, 1995; Nishikawa, 1997, 1998a, b):

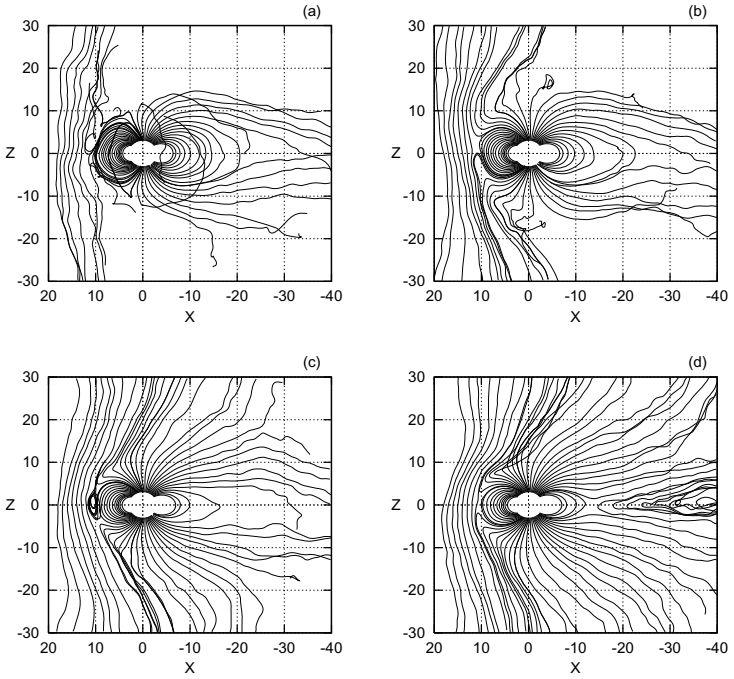

Fig. 5. Magnetic field lines in the xz plane containing the dipole center at step (a) 1024, (b) 1088, (c) 1216, and (d) 1280. The magnetic field lines are traced from near the Earth ($r = 3\Delta$ ($\approx 3R_E$)) and subsolar line in the dayside and the magnetotail. Some magnetic field lines are moved toward dawn or duskward. The tracing was terminated due to the preset number of points or the minimum strength of total magnetic field.

(1) Fresh particles representing the incoming solar wind (unmagnetized in our test run) are continuously injected across the yz plane at $x = x_{\min}$ with a thermal velocity plus a bulk velocity in the $+x$ direction; (2) thermal solar particle flux is also injected across the sides of our rectangular computation domain; (3) escaping particles are arrested in a buffer zone, redistributed there more uniformly by making the zone conducting in order to simulate their escape to infinity, and finally written off. We use a simple model for the ionosphere where both electrons and ions are reflected by the Earth dipole magnetic field. Effects of a conducting ionospheric boundary will be developed in future simulations. The effects of the Earth rotation are not included.

For the fields, boundary conditions were imposed just outside these zones (Buneman *et al.*, 1993, 1995; Nishikawa *et al.*, 1995; Nishikawa, 1997, 1998a, b): radiation is prevented from being reflected back inward, following Lindman's ideas (Lindman, 1975). The lowest order Lindman approximation was found adequate: radiation at glancing angles was no problem. However, special attention was given to conditions on the edges of the computational box.

In order to bring naturally disparate time scale and space scale closer together in this simulation of phenomena dominated by ion inertia and magnetic field interaction, the natural electron mass was raised to 1/16 of the ion mass and the velocity of light was lowered to twice the incoming solar wind velocity. This means that charge separation and kinetic phenomena are included qualitatively but perhaps not with quantitative accuracy. Likewise, radiation-related phenomena (e.g., whistler modes) are included qualitatively.

The first test exploring the solar wind-magnetosphere interaction was run on the CRAY-YMP at NCAR using a modest 105 by 55 by 55 grid and only 200,000 electron-ion pairs (Buneman *et al.*, 1993). We also have reported on our second test run on the CRAY-2 at NCSA using a larger 215 by 95 by 95 grid and about 1,500,000 electron-ion pairs (Buneman *et al.*, 1995). Initially, these fill the entire box uniformly and drift with a velocity $v_{\rm sol} = 0.5c$ in the $+x$ direction, representing the solar wind without an interplanetary magnetic field (IMF). The electron and ion thermal velocities are $v_{et} = (T_e/m_e)^{1/2} = 0.2c$, and $v_{it} = (T_i/m_i)^{1/2} = 0.05c$ ($= v_s = (T_e/m_i)^{1/2}$), respectively, while the magnetic field is initially zero. A circular-like current generating the dipole magnetic field is increased smoothly from 0 to a maximum value reached at step 65 and kept constant at that value for the rest of the simulation. The center of the current loop is located at (70.5Δ, 47.5Δ, 48Δ) with the current in the xy-plane and the axis in the z-direction. The initial expansion of the magnetic field cavity is found to expel a large fraction of the initial plasma. The injected solar wind density is about 0.8 electron-ion pairs per cell, the mass ratio is $m_i/m_e = 16$, and $\omega_{pe}\Delta t = 0.84$.

The primary purpose of this paper is to present a visualization technique that provides the topology of three-dimensional magnetic field reconnection. In this study, we determine the three-dimensional topology of the magnetic field uniquely. The temporal evolution of the global magnetic field topology reveals the topology that enables the magnetic fields reconnect. The visualization technique is important for us to determine whether the entire physical phenomenon is supercritical or subcritical by varying some solar wind parameters that can be considered as the external control parameters. Here we can choose a southward IMF

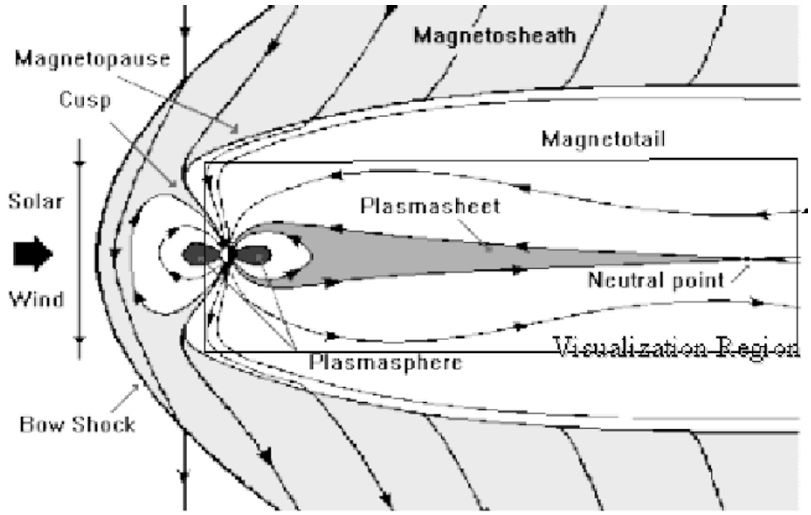

Fig. 6. The region which is visualized in the magnetotail is indicated by the rectangular box.

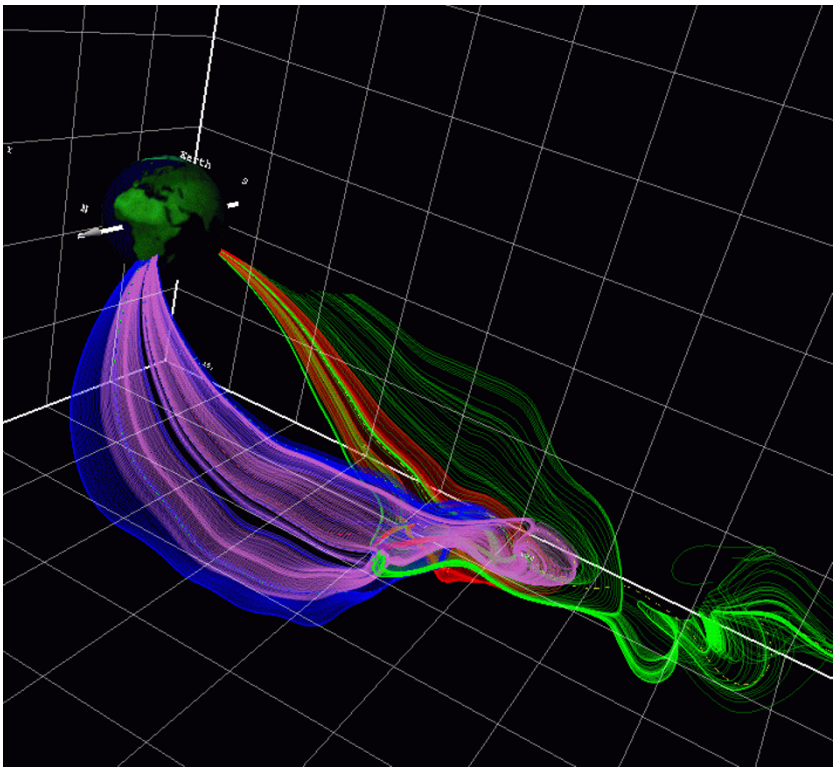

Fig. 7. Three-dimensional topology of magnetic field in the magnetotail region in Fig. 5(c). All characteristic surfaces that determine the three-dimensional topology are connected to the Earth's dipole except one.

$B_z{}^{\mathrm{IMF}}$ as the external parameter for this purpose. However, as an initial study, we use only two values $B_z{}^{\mathrm{IMF}} = 0, -0.4$.

In this paper, we report the magnetic field topology near the magnetic reconnection region in the near-Earth magnetotail as shown in Figs. 5 and 6. Here we first show the conventional two-dimensional magnetic field line plotted in Fig. 5. In our simulation, at step 768 (Buneman *et al.*, 1995; Nishikawa *et al.*, 1995) a southward IMF ($B_z^{\mathrm{IMF}} = -0.4$) is switched on, and the southward IMF front reaches about $x = 120\Delta$ at step 1280 (Nishikawa, 1997, 1998a). The Alfvén velocity with this IMF is $v_A/c = 0.1(\bar{n}_i)^{-1/2} = 0.1$ for the average ion density $\bar{n}_i = 1$.

To display magnetic reconnection at the dayside magnetopause and in the magnetotail. Figure 5 shows the magnetic field lines in the noon-midnight meridian plane for four different times (Nishikawa, 1997, 1998a). (Geocentric solar magnetospheric (GSM) coordinates are used in Fig. 5.) At step 1024, the solar wind with the southward IMF starts to interact with the dipole magnetic field at the dayside magnetopause (Fig. 5(a)). Figure 5(b) shows the X point in two-

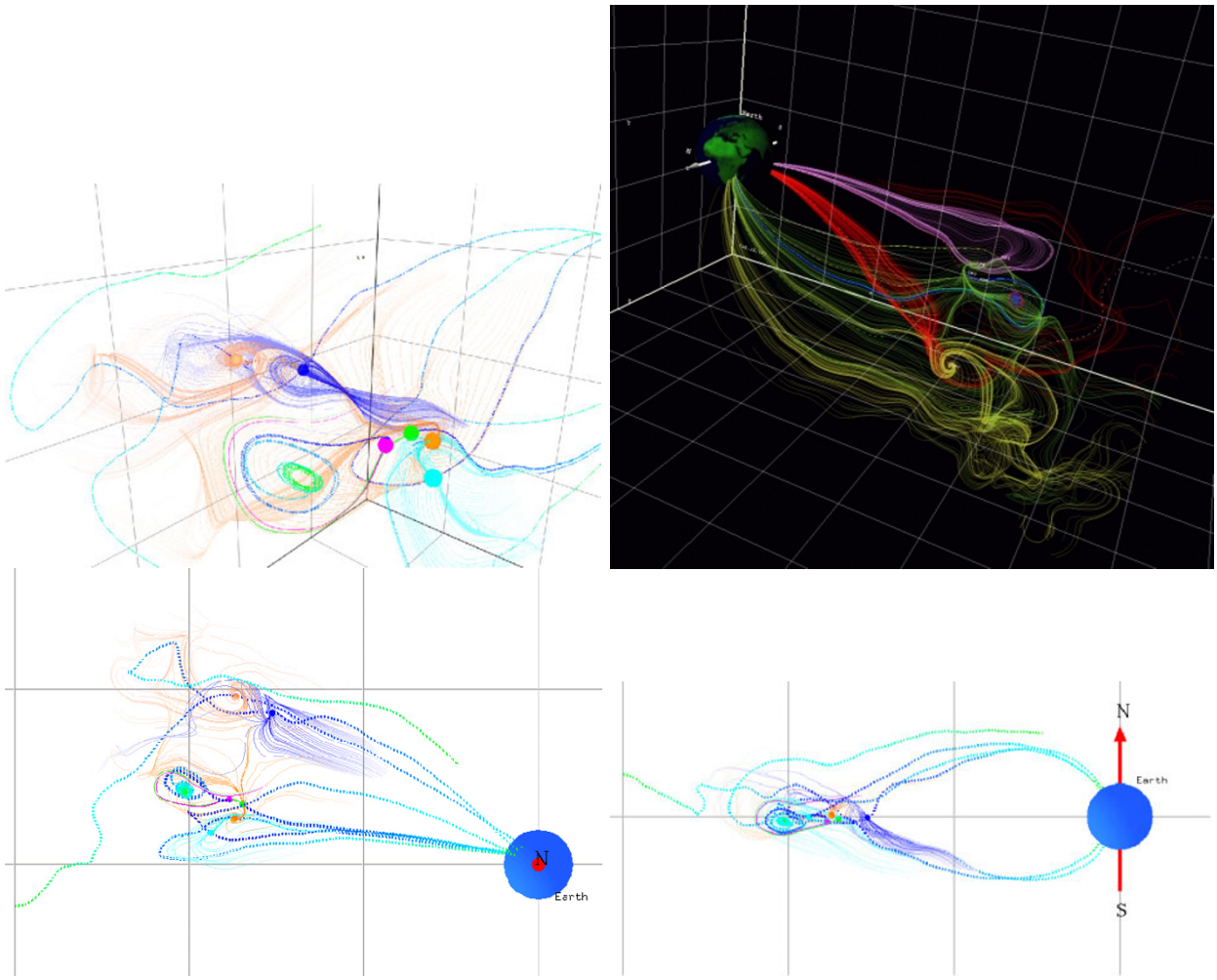

Fig. 8. Three-dimensional topology of magnetic fields in the magnetotail region at steps 1224 when the reconnection has not taken place. From the top left panel (clockwise) (a) Close-up view of six critical points that form a complicated three-dimensional "X-point" in space, (b) Wider view of the "X-point" region that shows the topology of magnetic field in three-dimension, (c) in the X-Y projection (viewed from north), and (d) in the X-Z projection (from the dawnside).

dimension at the magnetopause (step 1088) (Swift, 1996). The southward IMF is bent by the magnetosphere as shown in Fig. 5(c) (step 1216). Figure 5 displays an interesting magnetic structure near the subsolar magnetopause. Three-dimensional magnetic field shows that the reconnection occurs three-dimensionally in the dayside magnetopause along the equator (e.g., Walker and Ogino, 1996). At the same time, the stretched dipole magnetic fields are observed particularly in Fig. 5(c). Furthermore, the magnetic fields are stretched in the magnetotail, which leads to the growth of a tearing instability. Figure 5 shows the magnetic reconnection occurring at step 1280, with the X point in two-dimension located near $x = 85\Delta$ ($\approx -15R_E$) (Nishikawa, 1997, 1998a).

In this purpose, we have studied the three-dimensional topology of magnetic field using the TRISTAN particle simulation (Buneman, 1993) with the south IMF. Since it is difficult to determine the topology of the whole simulation domain due to numerical errors, we restrict the regions mainly in the magnetotail as shown in Fig. 6.

In the region indicated in Fig. 6, all the critical points found in the magnetotail and the Earth's dipole magnetic field region are hyperbolic and are not degenerated except at the center of the dipole. Therefore, the topology of the magnetic field is determined in the region including the Earth's magnetic dipole as shown in Figs. 7–10 using our algorithm discussed in Fig. 4. The three-dimensional magnetic field topologies shown in Figs. 7, 8, 9, and 10 are obtained at steps 1216, 1224, 1228, and 1236, respectively.

From Figs. 7 to 10, the magnetic field curves are all drawn from the critical points in the eigenvector directions. In reality, the curves start from the closest points which are a round-off error distance to the critical points since at the critical points magnetics are null. In these figures, we use 76 lines to represent the Σ-surfaces. The lines span out from the critical points on the surface. We do not tile these lined wire frame since the tilings prevent us from observing the details of the inside topology structure. The γ-lines are drawn as dotted arrow cone lines. If the Σ-surface lines span out as a spiral the critical points have the complex eigenvalues. Hence these critical points are types A_s or B_s, if not, the critical points have real eigenvalues and they are types A or B. If the Σ-surface lines goes to the earth north pole, the critical points are types A or A_s. Hence if the Σ-surface

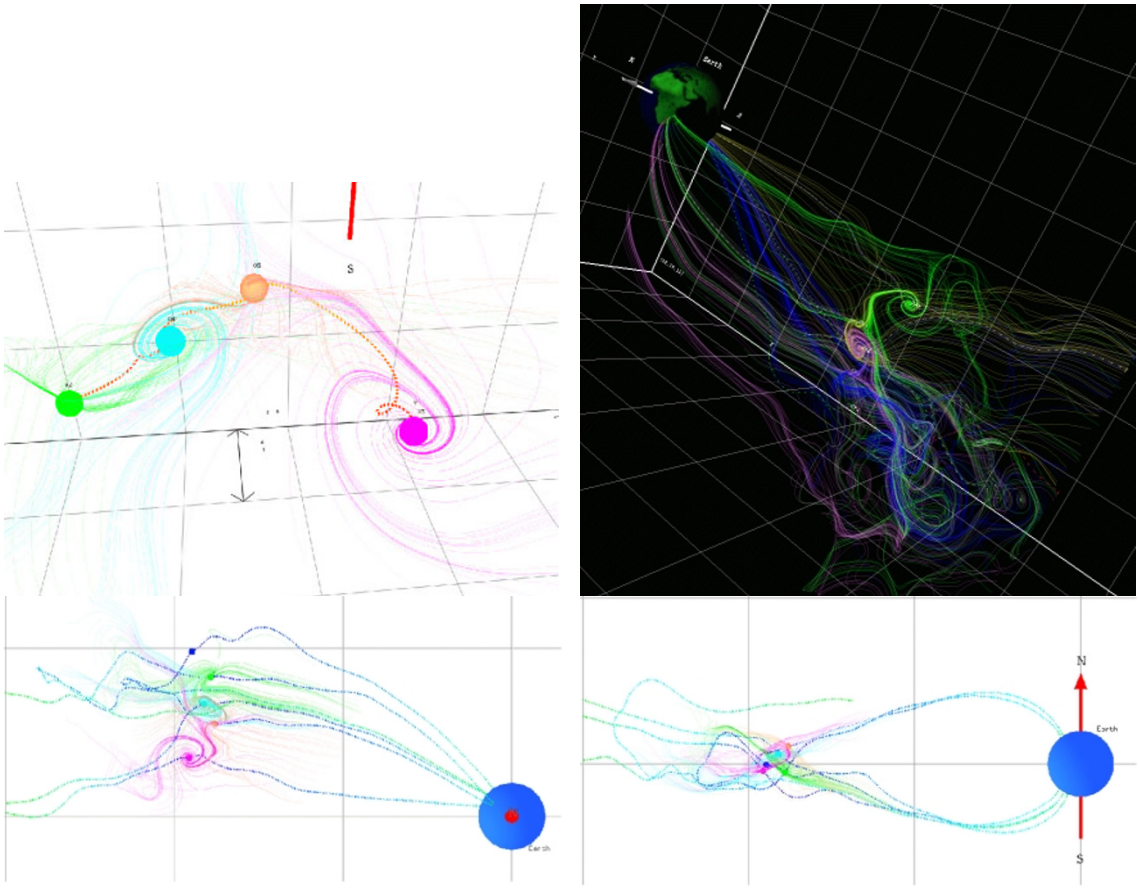

Fig. 9. Three-dimensional topology of magnetic field in the magnetotail region at step 1228 when the reconnection is about to take place. From the top left panel (clockwise) (a) Close-up view of six critical points that form a complicated three-dimensional "X-point" in space, (b) Wider view of "X-point" region that shows the critical topology of magnetic field in three-dimension, (c) in the X-Y projection (from north), and (d) in the X-Z projection (from the dawnside).

lines goes to the earth south pole, the critical points are types B or B_s. We can also judge the types of the critical points observing the γ-lines. If they go to the south pole or the north pole, the critical points are types A or A_s, or types B or B_s, respectively.

Figure 7 is obtained at step 1216, which corresponds to the magnetic field configuration shown in Fig. 5(c). All surfaces shown in this figure are Σ-surfaces, and are also called the separation surfaces that are spanned by the two eigenvectors that have the same sign in the real part of eigenvalues. However, it should be noted that many Σ-surfaces in this figure are not surfaces and rather a cylinder or cones that are extended from the critical points and are terminated in the Earth's dipole. In this figure, there exist four critical points in the visualized region. Three of them are mutually connected, which result in forming a complex three-dimensional "X-point" in the magnetotail. Except both a Σ-surface and a γ-line, all characteristic surfaces are connected to the Earth's north pole or south pole. As shown in Fig. 7, the γ-line originated from this exceptional critical point extends (not earthward) and is connected to the southward IMF in this simulation.

After 8 steps later at step 1224, the reconnection has not yet started. However, some critical changes in topology seem to occur as indicated in Fig. 8. The cylindrical Σ-surfaces that are connected and terminated in the Earth's dipole are now expanded significantly tailward. The four critical points are split into 6 critical points, which form two separated groups of critical points. In each group, one major critical point exists. Their Σ-surfaces are spiraled from the Earth-direction towards the magnetotail direction. Such a topology creates the so called "neutral line" between two groups of critical points and makes the open magnetic field lines or IMF to penetrate inside the magnetotail.

Less than four steps later (step 1228), the reconnection is suddenly taking place and the topology has been changed globally as shown in Fig. 9. At this time the IMF is penetrated and connected to three γ-lines and one Σ-surface is spanned toward the outside magnetotail.

In Fig. 10, the reconnection has fully taken place and the separated groups of six critical points shown in Fig. 9 have moved apart further. Thus more IMFs can penetrate into the center of the magnetotail.

To sum up these topology changes in magnetotail in time that are indicated as Figs. 8 to 10 in sequence, the critical points split into two groups on the plasma sheets (xy plane), spread in dawn-dusk y-direction, and shrink in day-night x-direction towards the Earth as time elapses. Thus a critical magnetic field topology that enables the global change of the topology is formed. Our hypothesis is that before the

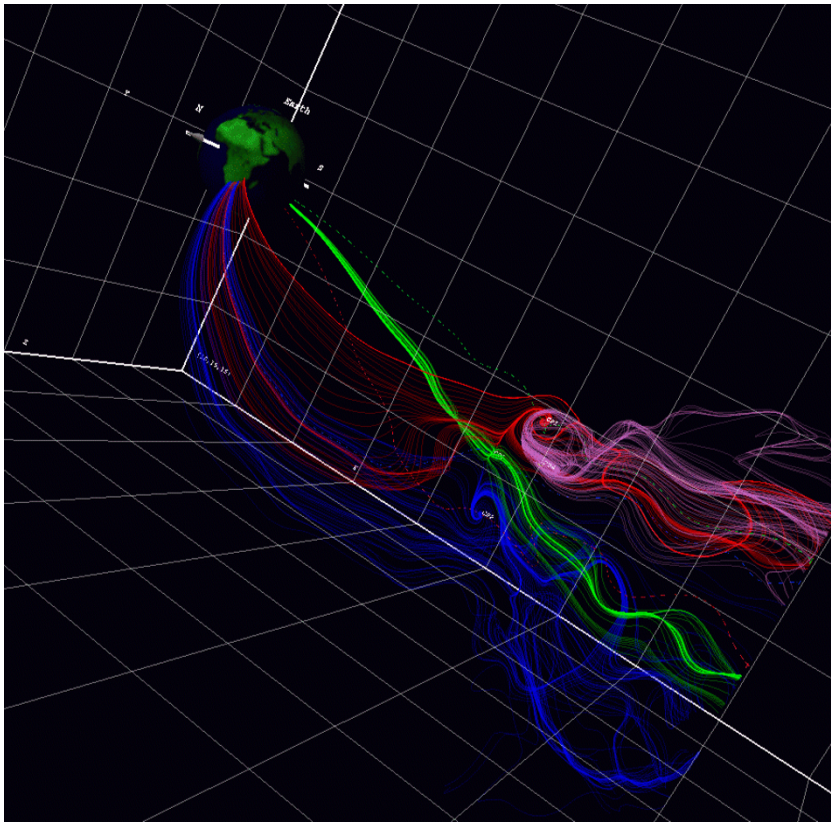

Fig. 10. Three-dimensional topology of magnetic field in magnetotail region at step 1236 when the reconnection is fully taking place.

global change of the magnetic field in the magentotail a critical topology exists to let the magnetic field inside the magnetosphere connect to the outside magnetic fields, i.e. IMFs, through the saddle points. However, the physical explanations of this topology are still under investigation.

4. Conclusions

In the present paper, we have successfully visualized the magnetic field topology in the magnetotail using the numerical data sets obtained by the three-dimensional full electromagnetic particle simulation (Nishikawa, 1997, 1998a). In our visualizations, the three-dimensional magnetic field topology in the magnetotail region is uniquely determined using our method described in Fig. 4. Through Figs. 7–10 we have presented the global and temporal changes of the magnetic field topology. It should be noted that the global changes of the magnetic field topology reveal the reconnection in plasma physics although this view or reconnection is not universally accepted. Since the field topology is uniquely determined by the eigenvalues of the critical points as shown in Figs. 7–10, we have examined that the magnetic field topology has been globally changed and the IMF has been penetrated into the magnetotail. There are 4 step intervals between Figs. 8 and 9 and the global changes of the magnetic field have taken place between these two time steps. Assuming the changes occur very slowly, one step before the global change of the topology is important. If the whole system is in steady state, we call it is in a critical state. Examining the magnetic field topology in Fig. 8, the critical points are split into two isolated groups and form a

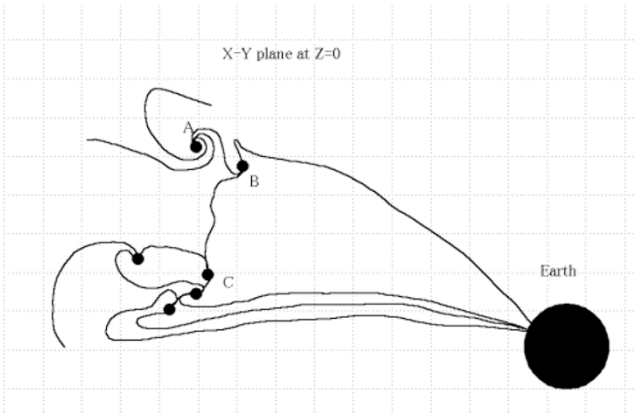

Fig. 11. Schematic view of the connected magnetic field topology at the x-y plane at $z = 0$ in the GSM coordinate at step 1224.

trapezoidal-like region on the xy plane at $z = 0$ in the GSM coordinate as shown in Fig. 11. In this figure, all critical points are close at $z = 0$ plane and the point A is connected to the point C through the point B, which is corresponds to the so called "neutral line." The important point here is that if the critical point at B or C vanishes or is split and the trapezoidal-like region is destroyed, the IMF or open magnetic field lines can penetrate and the reconnection can take place. We should note here that due to the low number of particles in one cell in our simulation, our particle simulations are very noisy although we are observing the magen-

tic field that is solved using the finite differenced Maxwell equations. Thus the topology is still correct in the sense of magnetic vector field topology solved using the finite differenced method. However, locations or the number of the critical points, or time behavior of them may be sensible to the noise level and is not a one simulated by the MHD model although they still observe the topology rules between them. Further investigations are necessary in order to clarify the topological changes associated with the magnetic reconnection and will be discussed in elsewhere using magnetic field data with better spatial and temporal resolutions.

References

Arnold, V. I., Ordinary differential equation, Springer, 1981.

Buneman, O., TRISTAN: The 3-D, E-M particle code, in *Computer Space Plasma Physics, Simulation Techniques and Software*, edited by H. Matsumoto and Y. Omura, pp. 67–84, Terra Sci., Tokyo, 1993.

Buneman, O., K.-I. Nishikawa, and T. Neubert, Solar wind-magnetosphere interaction as simulated by a 3D EM particle code, *Space Plasmas: Coupling Between Small and Medium Scale Processes*, Geophys. Monogr. Ser., vol. 86, edited by M. Ashour-Abdalla, T. Chang, and P. Dusenbery, pp. 347–352, AGU, Washington, D.C., 1995.

Lau, Y.-T. and J. M. Finn, Three-dimensional kinematic reconnection in the presence of field nulls and closed field lines, *Astrophys. J.*, **88**, 672–691, 1990.

Lindman, E. L., Free-space boundary conditions for the time dependent wave equation, *J. Comp. Phys.*, **18**, 66–78, 1975.

Nishikawa, K.-I., Particle entry into the magnetosphere with a southward IMF as simulated by a 3-D EM particle code, *J. Geophys. Res.*, **102**, 17,631–17,641, 1997.

Nishikawa, K.-I., Reconnections at near-earth magnetotail and substorms studied by a 3-D EM particle code, *Geospace Mass and Energy Flow*, edited by J. L. Horwitz, W. K. Peterson, and D. L. Gallagher, AGU Geophys. Monograph, **104**, pp. 175–181, 1998a.

Nishikawa, K.-I., Particle entry through reconnection grooves in the magnetopause with a dawnward IMF as simulated by a 3-D EM particle code, *Geophys. Res. Lett.*, **25**, 1609–1612, 1998b.

Nishikawa, K.-I., O. Buneman, and T. Neubert, Solar Wind-Magnetosphere Interaction as Simulated by a 3-D EM Particle Code, *Astrophys. Space Sci.*, **227**, 265, 1995, also in *Plasma Astrophysics and Cosmology*, edited by A. T. Peratt, pp. 265–276, Kluwer Academic Pub., 1995.

Swift, D. W., Use of a hybrid code for global-scale plasma simulation, *J. Comp. Phys.*, **126**, 109–121, 1996.

Walker, R. J. and T. Ogino, A global magnetohydrodynamic simulation of the origin and evolution of magnetic flux ropes in the Magnetotail, *J. Geomag. Geoelectr.*, **48**, 765–780, 1996.

D. Cai (e-mail: cai@is.tsukuba.ac.jp), Y. Li, T. Ichikawai, C. Xiao, and K. Nishikawa